

Experimental and theoretical study of electron-impact ionization of atomic ions in the Sm isonuclear sequence

K. Aichele, W. Arnold, D. Hathiramani, F. Scheuermann, and E. Salzborn
Institut für Kernphysik, University of Giessen, D-35392 Giessen, Germany

D. M. Mitnik and D. C. Griffin
Department of Physics, Rollins College, Winter Park, Florida 32789

J. Colgan and M. S. Pindzola
Department of Physics, Auburn University, Auburn, Alabama 36849
 (Received 27 April 2001; published 3 October 2001)

Experimental measurements and theoretical calculations of absolute cross sections are carried out for the electron-impact ionization of atomic ions in the Sm rare-earth-metal isonuclear sequence. Absolute cross sections for Sm^{q+} ions for $q=1-12$ were measured using the electron-ion crossed-beam technique and calculated with the configuration-average distorted-wave method for the charge states $q=4-12$. The theory includes both direct ionization and excitation-autoionization contributions, and includes transitions from both ground and metastable levels. We present the cross sections in an electron-impact energy range from threshold up to 1000 eV for all Sm ions up to Sm^{12+} . These systems are extremely complex, but the configuration-average method, when combined with statistical averaging of the cross sections over the many levels, provides results that are in overall good agreement with the experimental measurements. The single-ionization cross sections are dominated by contributions from indirect mechanisms of excitation-autoionization in the low-energy region.

DOI: 10.1103/PhysRevA.64.052706

PACS number(s): 34.80.Dp, 34.70.+e

I. INTRODUCTION

One of the most important atomic collision processes is the electron-impact ionization of atomic ions. These cross sections are required for modeling the structure and dynamics of laboratory and astrophysical plasmas. Due to the lack of an extensive experimental database, theoretical cross sections are often used in the calculation of different plasma parameters.

For one-electron systems [1] or light ions [2], experiment and theory are in very-good agreement. For these ions the dominant mechanism for single ionization is simply direct (knockout) ionization. However, indirect mechanisms can also play an important role in electron-impact ionization. Experiments by Peart and Dolder [3] on singly charged ions and by Falk *et al* [4] on multiply charged ions clearly demonstrate the importance of indirect ionization mechanisms proceeding via inner-shell excitation and subsequent autoionization. A summary of the theoretical work and comparisons with experiments of these indirect processes is provided in Ref. [5]

The excitation-autoionization (EA) process is generally characterized by a steplike feature in the total ionization cross section. This mechanism is evident especially for those targets with one or more electrons outside a closed $l \geq 1$ subshell. For Li-like ions, this has been studied extensively, experimentally and theoretically. In this case, the electronic structure is complex enough to supply a variety of indirect processes, yet simple enough to allow detailed, theoretical calculations [6–10] and to identify individual ionization mechanisms in the experimental data [11–14]. The work on Li-like ions and also Mg-like ions [15] demonstrates that

excitation-autoionization processes become more important as the charge state increases.

Studies of isoelectronic sequences have been carried out mostly for ions with one or two electrons outside closed shells. The purpose is to gain insight into fundamental processes contributing to the electron-impact ionization of ions and into their dependence on the charge of the ion. Cross-section data is also required along an isonuclear sequence. Such data is needed for studies of charge-state time evolution in plasmas or studies to determine the distance to the plasma edge.

However, the effort in calculating direct ionization and especially EA cross sections increases with the number of the electrons. For intermediate and heavy atomic ions, substantial contributions to single-ionization arise from indirect ionization processes. In theoretical studies of the Cu-like isoelectronic sequence [16], the EA contributions are found to dominate the direct ionization. This increasing importance can also be observed in studies of the alkaline earth series, namely, Be^+ , Mg^+ , Ca^+ , Sr^+ , and Ba^+ [17–19]. Other crossed-beam measurements have mapped out complex resonance structures for the heavy metal ions Cs^+ , Ba^{2+} , Ba^{3+} , La^{2+} , and La^{3+} [20–22].

In neutral rare-earth-metal atoms the $4d$ photoabsorption spectra are dominated by a broad $4d \rightarrow 4f$ excitation. Due to the strong $4d$ resonances we also expect $4d$ EA contributions in the cross section of the electron-impact ionization of rare-earth-metal ions. The complex electron structure of few-times ionized heavy elements makes detailed analysis of the cross section of Sm ions very difficult, since there are numerous strong excitation channels that can potentially create a rich variety of observable indirect ionization effects. The

study of a rare-earth-metal isonuclear sequence such as Sm, with a half-filled $4f$ shell, has other merits. There exists almost no measurements or theoretical calculations for electron-impact ionization for such complex ions. These studies provide an important test of theoretical predictions for ions with open $4d$, $5p$, and $4f$ shells. By comparison of experimental measurements and theoretical calculations one can test our understanding of complex atomic structure and dynamics. Furthermore, the rare-earth-metal elements produce one of the maxima in the distribution curve of the elements in the sun [23], so knowledge of the cross sections of Sm ions can improve the modeling of astrophysical plasmas.

The remainder of this paper is structured as follows. In Sec. II we describe the crossed-beams experiment method. In Sec. III we review distorted-wave theory as applied to the electron-impact ionization of atomic ions. In Sec. IV we show the experimental results for Sm^+ up to Sm^{12+} , while in Sec. V we present a comparison between experimental and theoretical results. In Sec. VI we give a brief summary.

II. EXPERIMENTAL TECHNIQUE

The measurements were performed at the electron-ion crossed-beams facility in Giessen. The technique used has been described in detail previously [12,24]. The Sm ions were produced in a 10 GHz electron cyclotron resonance (ECR) ion source using an evaporation oven. Ion currents up to 15 nA of $\text{Sm}^+ - \text{Sm}^{13+}$ ions with energies of $q \times 10$ keV have been obtained. The comparatively low-ion current was caused by the unfavorable isotope distribution of samarium, where ^{152}Sm is the isotope with the largest partition (26.7%) in the natural mixture. In most cases, the isotope ^{152}Sm was used for the measurements. Investigating the Sm^{4+} and Sm^{8+} ionization cross sections, measurements were performed with the isotope ^{154}Sm (22.7%). The isotope ^{147}Sm (15%) was used for the experiments with Sm^{9+} and Sm^{11+} ions. This was necessary because for these charge states the mass-to-charge ratio of ^{152}Sm is very similar to the ratio from impurity ions like OH^+ or N^+ , which are also produced in the ECR ion source and cannot be separated magnetically from each other.

After magnetic analysis and tight collimation to typically $1.5 \times 1.5 \text{ mm}^2$ the ions were crossed with an intense electron beam at an angle of 90° . The electron gun supplies a ribbon-shaped electron beam with energies between 10 and 1000 eV and currents up to 430 mA [25]. After the interaction, the product ions were separated magnetically from the parent-ion beam and detected by a single-particle detector. The parent-ion beam was collected in a large Faraday cup. Absolute cross sections were obtained by employing the dynamic crossed-beam technique described in detail earlier [26], where the electron beam is moved vertically through the ion beam with simultaneous registration of the ionization signal and both beam currents. The total experimental uncertainty of the measured cross sections is typically 8% at the maximum. It results from the square sum of signal counting statistics at 95% confidence level and nonstatistical errors of about $\pm 7.8\%$ (ion-detection efficiency $\pm 3\%$; ion and elec-

tron currents $\pm 5\%$; ion and electron velocity $\pm 1\%$ and channel width $\pm 1\%$).

III. CALCULATIONAL PROCEDURE

Major contributions to the electron-impact single-ionization cross section are made by the following two processes:

$$e^- + \text{Sm}^{q+} \rightarrow \text{Sm}^{(q+1)+} + e^- + e^-, \quad (1)$$

and

$$e^- + \text{Sm}^{q+} \rightarrow (\text{Sm}^{q+})^* + e^- \rightarrow \text{Sm}^{(q+1)+} + e^- + e^-, \quad (2)$$

where the Sm ion has charge q . The first process is direct ionization while the second is EA. Assuming the two processes occur independently and do not interfere, the total ionization cross section is given by

$$\sigma_I(g \rightarrow f) = \sigma_{DI}(g \rightarrow f) + \sigma_{EA}(g \rightarrow f), \quad (3)$$

where $\sigma_{DI}(g \rightarrow f)$ is the direct ionization cross section and $\sigma_{EA}(g \rightarrow f)$ is the excitation-autoionization cross section from an initial level g of the N -electron ion to a final level f of the $(N-1)$ -electron ion. The excitation-autoionization cross section through inner-shell excitation to an intermediate autoionizing level j is given by:

$$\begin{aligned} \sigma_{EA}(g \rightarrow f) &= \sum_j \sigma_E(g \rightarrow j) \left[\frac{A_a(j \rightarrow f)}{\sum_k A_a(j \rightarrow k) + \sum_i A_r(j \rightarrow i)} \right] \\ &\equiv \sum_j \sigma_E(g \rightarrow j) B_a(j \rightarrow f), \end{aligned} \quad (4)$$

where $\sigma_E(g \rightarrow j)$ is the excitation cross section from level g to level j , $A_a(j \rightarrow k)$ is the autoionizing rate from level j to level k , $A_r(j \rightarrow i)$ is the radiative rate from level j to any lower-energy level i , and $B_a(j \rightarrow f)$ is the branching ratio for autoionization from level j to level f , defined by the term in large square brackets.

The branching-ratio value is dictated by the ratio of the autoionization to the radiative rates. If the level is not autoionizing, the branching ratio is zero. We assume in our calculations a unitary branching ratio for those configurations lying above the first ionization limit. This approximation is very good for neutrals and weakly ionized atoms, where the radiative transition rates are much smaller than the autoionization rates. The A_r rates grow approximately as $(q+1)^4$ for $\Delta n=1$ transitions, q being the ion-charge number. On the other hand, the autoionization rates are nearly independent of q , and therefore, we can expect a decrease in the branching ratios for higher ionized ions. Thus, our approximation could lead to overestimations in the total ionization for the more highly ionized ions. We have calculated the configuration average rates for Sm^{12+} , as described in the following sections, and found that the autoionization rates are still more dominant. This supports our assumption, but

one has to keep in mind that the configuration average picture can be different than the detailed level-by-level behavior.

The direct ionization and the electron-impact excitation cross sections are calculated in an configuration-average distorted-wave approximation (CADW), which is described in detail elsewhere [27]. Due to the complexity of the atomic structure of the ions studied in this work, the configuration-average method is the only feasible approach for a practical calculation. In the CADW approximation, the first-order scattering amplitude for either the ionization or excitation process is averaged over all states of an initial configuration and summed over all states of a final configuration. The bound-state energies and the atomic orbitals for the many configurations are generated using the radial wave-function code developed by Cowan [28]. These radial wave functions are solutions to the Hartree-Fock equations. The continuum orbitals needed to evaluate the Coulomb matrix elements were calculated in a local distorting potential constructed in a semiclassical exchange approximation [29].

As we will show in the following sections, details of the levels belonging to the ground and autoionizing configurations are needed for some particular cases. We calculate the atomic structure of these inner-shell excited levels by using the HULLAC package [30]. In this package, the detailed level energies are calculated using the fully relativistic multiconfigurational RELAC code [31], based on the parametric potential model [32]. The central potential is introduced as an analytic function of screening parameters that are determined by minimizing the first-order relativistic energy of a set of configurations.

IV. EXPERIMENTAL RESULTS

Experimental results of the electron-impact ionization cross section of Sm^+ to Sm^{12+} are shown in Figs. 1–3. The error bars indicate the total experimental uncertainties of the absolute measurements. The statistical uncertainties of typically 1% are smaller than the plotted symbols in each of the figures.

The general trend of the curves is summarized in Fig. 4 in which the maximum value of the cross section is plotted as a function of the charge q of the different Sm^{q+} ions. The shape of this curve can be understood as the result of the competition of the two ionization mechanisms. The direct ionization, which decreases rapidly with the ion charge, is the dominant ionization process for the low-charge ions. Therefore, the maximum of the cross section decreases from 303 Mb for $q=1$ to 42 Mb for $q=5$. The ionization cross sections shown in Fig. 1 are also relatively smooth curves, reflecting the dominance of the direct ionization over the indirect processes. The excitation-autoionization process, on the other hand, has a different behavior along the isonuclear sequence. This is the dominant mechanism for the ionization of higher-charge ions. In these cases, the main reason for the decrease of the maximum cross section, is the closing of the autoionization channels.

We can extract also information regarding the presence of ions in metastable states from the experimental results dis-

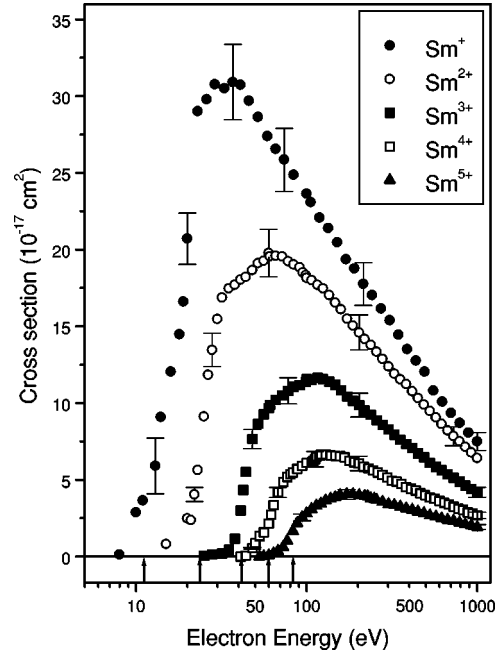


FIG. 1. Total cross sections for the electron-impact single ionization of $\text{Sm}^+ - \text{Sm}^{5+}$. The sample error bars represent the total experimental uncertainties and the arrows indicate the threshold energies for ionization from the ground state of the respective ions.

played in Figs. 1–3. The vertical arrows in these figures, mark the threshold energies for ionization. These energies are taken from spectroscopic data ($\text{Sm}^+ - \text{Sm}^{3+}$ [33]) or calculated by the CADW theory ($\text{Sm}^{4+} - \text{Sm}^{12+}$). The onset of the respective electron-impact ionization cross sections are in most of the cases below the calculated ionization threshold for the ground state, indicating the possible presence of metastables. However, this is not the only possible explanation. As an example, in Sm^{4+} , the experimental cross section begins to rise at 45 eV whereas the first level of the Sm^{5+} has an energy of 61 eV. However, the 107 levels belonging to

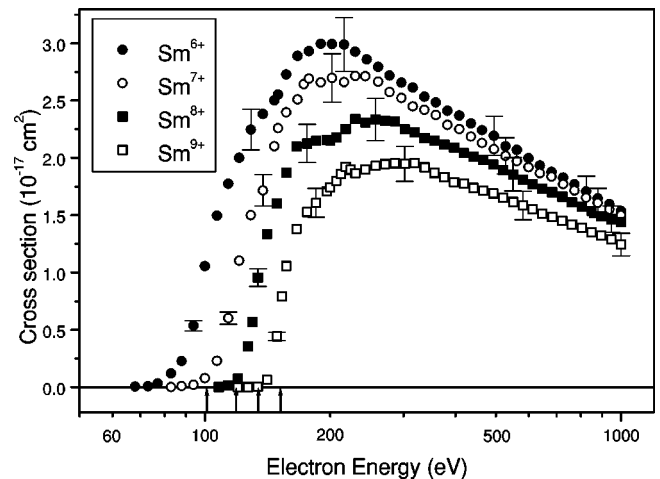


FIG. 2. Total cross sections for the electron-impact single ionization of $\text{Sm}^{6+} - \text{Sm}^{9+}$. The sample error bars represent the total experimental uncertainties and the arrows indicate the threshold energies for ionization from the ground state of the respective ions.

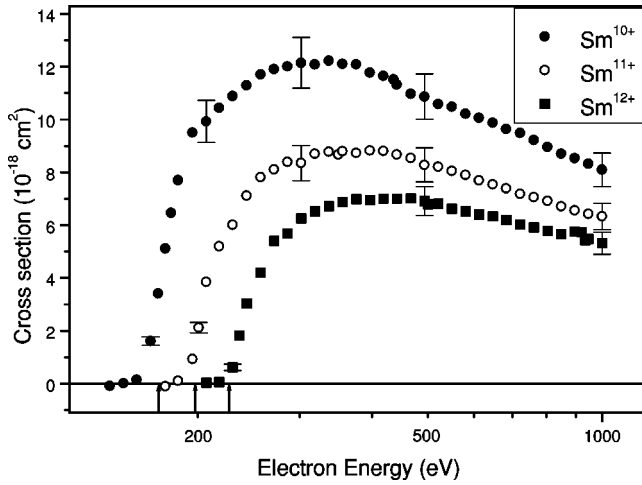


FIG. 3. Total cross sections for the electron-impact single ionization of $\text{Sm}^{10+} - \text{Sm}^{12+}$. The sample error bars represent the total experimental uncertainties and the arrows indicate the threshold energies for ionization from the ground state of the respective ions.

the ground configuration cover an energy range of about 24 eV making possible the ionization from many of these levels at lower energies than the average-configuration threshold.

V. COMPARISON BETWEEN THEORY AND EXPERIMENTS

A. General considerations

For the ions considered in this study, the $4d$ and $5s$ orbitals are closed, and the remaining electrons are in the $5p$ and $4f$ orbitals. The order in which these orbitals are filled is dependent on the particular ion and therefore care must be taken in the calculation of the structure of the lower configurations. For ions with a low degree of ionization, the $5p$ orbital is filled before the $4f$, but the situation changes when the degree of ionization increases. For example, the ground configuration for Sm^{4+} is $[\text{Kr}]4d^{10}5s^25p^64f^4$ but for

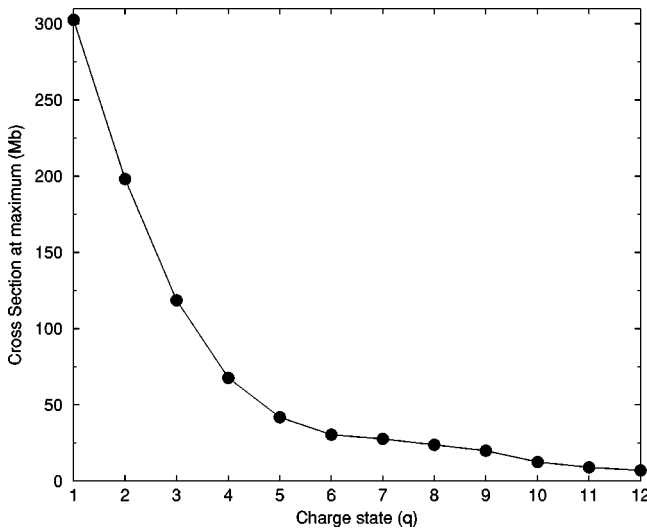


FIG. 4. Behavior of the total cross section maxima for the electron-impact single ionization of $\text{Sm}^{q+} - \text{Sm}^{12+}$.

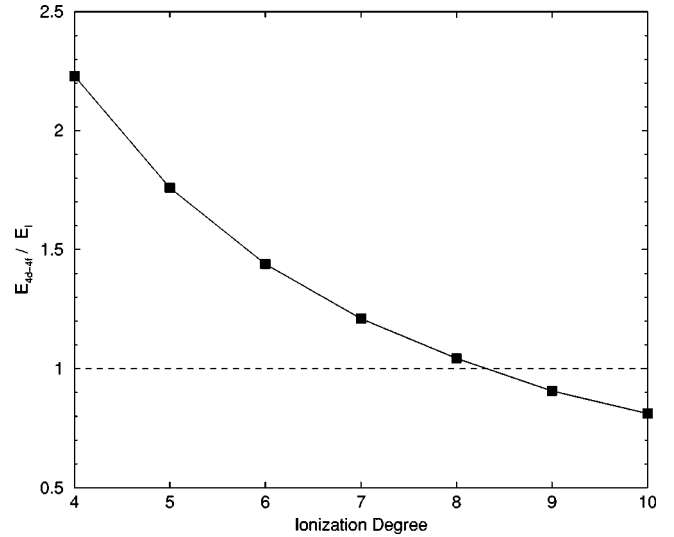


FIG. 5. Ratio between the average transition energy for inner-shell excitation from $4d^{10}5s^25p^n4f^m$ to the $4d^95s^25p^n4f^{m+1}$ configuration, and the first ionization energy E_I , as a function of the ionization degree in the Sm isonuclear sequence.

Sm^{10+} it is $[\text{Kr}]4d^{10}5s^24f^4$. For Sm^{12+} , the ground configuration is $[\text{Kr}]4d^{10}5s^24f^2$, but in this case, the energy of the $4f$ orbital is close to that of the $5s$ orbital; therefore, we also need to consider the $4d^{10}4f^4$ metastable configuration as potentially populated. Since the $4f$ and the $5p$ orbitals have the same parity and roughly the same energy, configuration interaction is also important. Therefore, the number of levels that must be considered in any detailed calculation is so large that, in some cases, even the angular-algebra calculation exceeds the capability of a standard computer. The only method that is feasible in these cases is the configuration-average approach. Previous calculations [34] show that the relative accuracy of this method increases as the number of levels in the configuration increases.

The intermediate autoionizing configurations that can contribute to the excitation-autoionization processes arise from transitions from the $4d$ and $4p$ orbitals, and in some cases, also from the $5s$ orbitals. The dominant transition is $4d-4f$ arising from excitations from $4d^{10}5s^25p^n4f^m$ to $4d^95s^25p^n4f^{m+1}$. In order to obtain insight into the importance of this transition along the isonuclear sequence, we analyze the relative energy of the inner-shell excited configurations, with respect to the ionization limit. Figure 5 shows the ratio of the average energy of the configurations $4d^95s^25p^n4f^{m+1}$ (E_{4d-4f}) to the average ionization energy E_I . It must be stressed that the picture given by the average configuration energies is only an approximate one. Indeed, the excited configurations contain a large number of levels, which are spread around the average of the configurations. Moreover, in several cases, the total collision excitation from the ground state to a particular configuration is dominated by only a few inner-shell excited levels, which have energy values that might be quite different from the configuration-averaged energy. We estimate that including the $4d-4f$ transition for Sm^{q+} ions, for ions with q higher than 5, will result in an overestimation of the cross section, due to the fact that

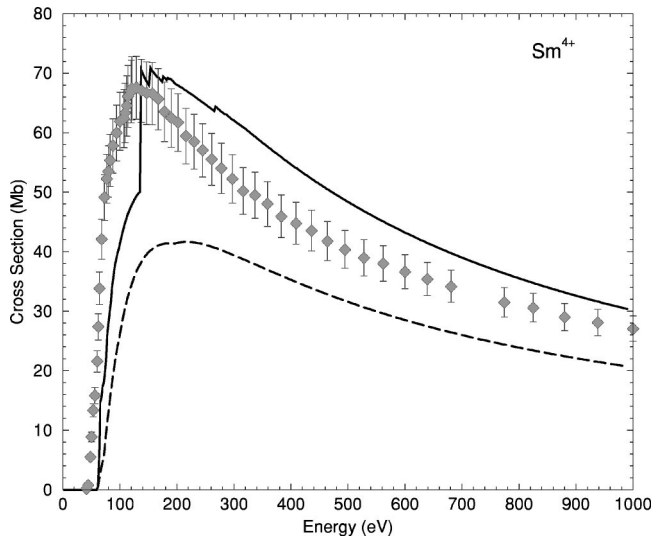


FIG. 6. Electron-impact cross section for the ionization of Sm^{4+} from the ground configuration $4d^{10}5s^25p^64f^4$. The dashed curve is the calculated direct ionization and the solid curve is the calculated total cross section. The diamonds are the experimental results. ($1.0 \text{ Mb} = 1.0 \times 10^{-18} \text{ cm}^2$.)

there are many levels of the excited configuration lying below the ionization limit. In the following we will discuss the comparison between the calculations and the experiment for some selected ions in this isonuclear sequence. We chose the cases for which the most-interesting physical effects are present.

B. Sm^{4+}

In Fig. 6 we compare configuration-average distorted-wave calculations with experimental measurements (solid diamonds). We present results for direct ionization (dashed line) that includes ionization from the $4f$, $5p$, $5s$, and $4d$ subshells, and for total ionization (solid line), including excitation autoionization. The ground configuration of Sm^{4+} is $[\text{Kr}]4d^{10}5s^25p^64f^4$ and the average ionization energy is 60 eV. The dominant direct-ionization path mechanism is the ionization of the six $5p$ electrons (with an average ionization potential of 72 eV), which produces a peak of 24 Mb at 173 eV. The next most-important contribution to direct ionization is from the four $4f$ electrons that gives a peak of 14 Mb at 210 eV.

For the excitation-autoionization calculations we include the inner-shell excitations $4d-4f$, $4d-5\ell$ ($\ell = d, f, g$), $4d-n\ell$ ($n = 6$ to 8 ; $\ell = s$ to g), $4p-4f$, $4p-5\ell$ ($\ell = d, f, g$), $4p-n\ell$ ($n = 6$ to 8 ; $\ell = s$ to g), $5s-4f$, $5s-5\ell$ ($\ell = d, f, g$), and $5s-n\ell$ ($n = 6$ to 8 ; $\ell = s$ to g). The main inner-shell transition is $4d-4f$, which has an average threshold of 135 eV, far above the ionization limit. Detailed calculations for the excited configuration show that it consists of 1878 levels, and that all the levels of the configuration are autoionizing. An additional important transition is the $5s-5d$ inner-shell excitation, which has an average energy of 55 eV. We performed detailed calculations for the $[\text{Kr}]4d^{10}5s^15p^64f^45d$ configuration, and the results show that among the 1954 levels, about 1100 lie above the ioniza-

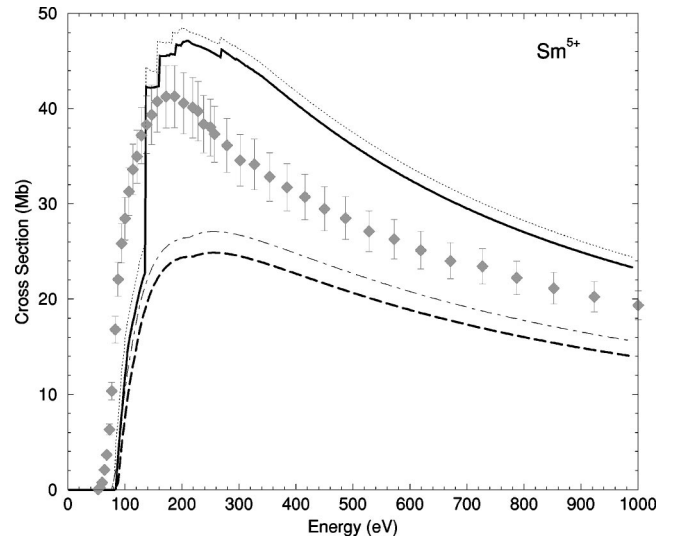


FIG. 7. Electron-impact cross section for the ionization of Sm^{5+} . The thick curves are transitions from the ground configuration $4d^{10}5s^25p^64f^3$: the dashed curve is the calculated direct ionization cross section and the solid curve is the calculated total ionization cross section. The fine-line curves are transitions from the metastable $4d^{10}5s^25p^54f^4$ configuration: the dot-dashed curve is the calculated direct ionization cross section and the dotted curve is the calculated total ionization cross section. The diamonds are the experimental results. ($1.0 \text{ Mb} = 1.0 \times 10^{-18} \text{ cm}^2$.)

tion limit. Therefore we determined the ratio of the sum of the statistical weights of the autoionizing levels to the total statistical weight of the configuration and then we multiplied the $5s-5d$ excitation cross section by the calculated value of this ratio of 0.51.

For the $[\text{Kr}]4d^{10}5s^15p^64f^45d$ configuration, we also calculated the statistically averaged energy of the levels lying above the ionization limit. We obtained 65 eV, and this was the energy position we assigned to the first peak in the total cross section shown in Fig. 6. It is worth pointing out that the configuration-averaged cross section gives a peak at one particular (the average) energy, while the actual physical cross section is spread over all the levels belonging to the configuration. Therefore, we expect the configuration average method to underestimate the cross section at energies below the average threshold, and to overestimate the cross section for energies above the threshold. Taking into account these factors, the agreement between the calculated cross section and the experimental values is good.

C. Sm^{5+}

In Fig. 7, we present results for the electron-impact ionization of Sm^{5+} including direct (dashed line) and total ionization (solid line), along with the experimental values (solid diamonds). The calculations include direct ionization from the $4f$, $5p$, $5s$, and $4d$ subshells. This case is very similar to Sm^{4+} ; however, the total cross section is about 40% smaller. The ground configuration of this ion is $[\text{Kr}]4d^{10}5s^25p^64f^3$ and the average ionization energy is 83 eV. The average ionization energy for the $5p$ electron is 88 eV, which is about 15 eV higher than the same ionization energy for the Sm^{4+} . The

direct ionization of the six $5p$ electrons produces a peak of 16 Mb at 194 eV, and the direct ionization of the $4f$ electrons has a maximum of 7 Mb at 296 eV. The reduction in the direct ionization cross sections in going from Sm^{4+} to Sm^{5+} is partially due to the increase in ionization energies, as well as presence of three, rather than four, $4f$ electrons in the ground-state configuration.

For the excitation-autoionization calculations, we included the same transitions as in Sm^{4+} . The main inner-shell transition is the $4d$ - $4f$, which has nearly the same excitation cross section as in Sm^{4+} . Furthermore, just as in the case of Sm^{4+} , the average threshold energy is 135 eV; it is far above the ionization limit, and the whole configuration is autoionizing. The $5s$ - $5d$ inner-shell excitation, also has the same average energy as for Sm^{4+} ; however, the ionization energy has increased sufficiently that all 759 levels of the $[\text{Kr}]4d^{10}5s^15p^64f^35d$ lie below the ionization limit, and this transition does not contribute to the EA cross section. This leads to an overall reduction in the indirect contribution to ionization for this ion, but it is important to note that the relative value of indirect to direct ionization actually increases.

The experimental results displayed in Fig. 7 show that the cross section begins at 56 eV, which is far below the theoretical threshold of 83 eV. However detailed calculations of the energy levels of the ground configuration $[\text{Kr}]4d^{10}5s^15p^64f^3$ for Sm^{5+} yield a spread of only 14 eV while the ground configuration $[\text{Kr}]4d^{10}5s^15p^64f^2$ of Sm^{6+} has a spread of only 10 eV. We also calculated the configuration-average ionization cross section from the metastable configuration $[\text{Kr}]4d^{10}5s^15p^54f^4$, which has 611 levels spread between 8 eV and 40 eV above the first level of the ground configuration. This cross section is displayed in the same figure with fine-line curves, which are similar to the cross sections from the ground state. Although we cannot provide a definitive explanation of this discrepancy in the ionization threshold, we believe that it is most likely due to the presence of metastable configurations in the ion beam.

D. Sm^{10+}

The ground configuration of Sm^{10+} is $[\text{Kr}]4d^{10}5s^24f^4$, has 107 levels, and an average ionization energy of 168 eV. Figure 8 shows the results of the direct (dashed line) and the total ionization (solid line), together with the experimental values (solid diamonds). Direct ionization calculations include ionization from the $4f$, $5s$, $4d$, and $4p$ subshells. However for this ion, the direct ionization cross section from the ten $4d$ electrons provides a larger contribution to the total ionization cross section than in Sm^{9+} .

For the excitation-autoionization calculations, we include the inner-shell excitations $4d$ - $4f$, $4d$ - $n\ell$ ($n=5$ to 8 ; $\ell=s$ to g), $4p$ - $4f$, and $4p$ - $n\ell$ ($n=5$ to 8 ; $\ell=s$ to g). All the $5s$ - nl excited levels are below the ionization limit. The main inner-shell transition is the $4d$ - $4f$, which again has an average threshold at 137 eV. We performed detailed calculations for the $[\text{Kr}]4d^{10}5s^14f^5$ configuration, and the results show that among the 1878 levels, about 300 lie above the ioniza-

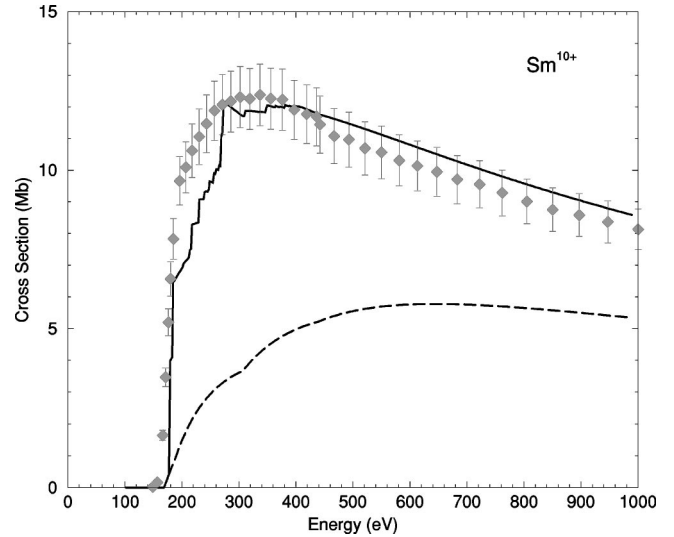


FIG. 8. Electron-impact cross section for the ionization of Sm^{10+} from the ground configuration $4d^{10}5s^24f^4$. The dashed curve is the calculated direct ionization cross section and the solid curve is the calculated total cross section. The diamonds are the experimental results. ($1.0 \text{ Mb} = 1.0 \times 10^{-18} \text{ cm}^2$.)

tion limit. We again calculated the ratio of the total number of states above the ionization limit to the total number of states for this configuration, as discussed previously, and obtained a value of 0.13. In order to include the $4d$ - $4f$ contribution in Fig. 8, we multiplied the excitation cross section by this ratio and positioned the peak at the average energy of those levels that are autoionizing.

E. Sm^{12+}

The ground state of Sm^{12+} is $[\text{Kr}]4d^{10}5s^24f^2$, which has 13 levels spread over 12 eV, and an average ionization potential of 229 eV. However, for this high degree of ionization, the energies of the $4f$ electrons are comparable with the energies of the $5p$ and the $5s$ electrons. Therefore, only a large detailed calculation that includes configuration interaction makes it possible to determine precisely the structure of the low-lying configurations. Among others, the lowest configurations are the $[\text{Kr}]4d^{10}5s4f^3$ that has 82 levels between 7 and 25 eV, the $[\text{Kr}]4d^{10}5s^24f5p$ with 12 levels between 15 and 25 eV, and the $[\text{Kr}]4d^{10}4f^4$ configuration with 107 levels between 21 and 50 eV. All these configurations contain levels that are metastable. In Fig. 9 we present the electron-impact ionization cross sections from the ground and the metastable $[\text{Kr}]4d^{10}4f^4$ configuration only. Results from the other metastable configurations lie between these two curves. Again, the largest direct ionization cross section is produced by the ten $4d$ electrons, followed by the ionization of the six $4p$ electrons. We also included ionization from the $4f$ electrons, and, where possible, ionization from the $5s$ electrons.

For the excitation-autoionization calculations, we included the inner-shell excitations $4d$ - $4f$, $4d$ - $n\ell$ ($n=5$ to 8 ; $\ell=s$ to g), $4p$ - $4f$, $4p$ - $n\ell$ ($n=5$ to 8 ; $\ell=s$ to g), $4s$ - $4f$, and $4s$ - $n\ell$ ($n=5$ to 8 ; $\ell=s$ to g). The largest excitation cross sections are the $4d$ - $4f$, $4d$ - $5p$, and the $4d$ - $5p$ transi-

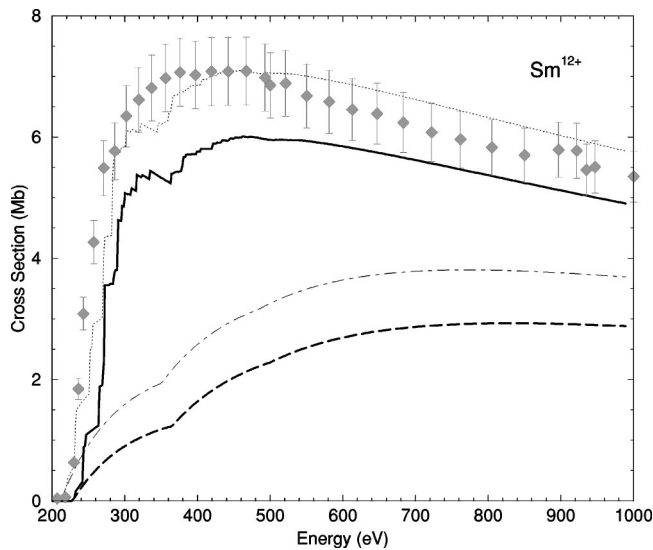


FIG. 9. Electron-impact cross section for the ionization of Sm^{12+} . The thick curves are transitions from the ground configuration $4d^{10}5s^2 4f^2$; the dashed curve is the calculated direct ionization cross section and the solid curve is the calculated total ionization cross section. The fine-line curves are transitions from the metastable $4d^{10}4f^4$ configuration: the dot-dashed curve is the calculated direct ionization cross section and the dotted curve is the calculated total ionization cross section. The diamonds are the experimental results. ($1.0 \text{ Mb} = 1.0 \times 10^{-18} \text{ cm}^2$.)

tions, which have average energies of 138 eV, 155 eV, and 199 eV, respectively. The excited configuration resulting from the $4d$ - $4f$ excitation is completely below the ionization limit. The $4d$ - $5p$ excited configuration has only about 25 autoionizing levels, out of a total number of 626 levels. The $4d$ - $5d$ excited configuration has 992 levels, of which only about 80 are autoionizing. The ratios of autoionizing states to the total number of states for these configurations are 0.03 and 0.06, respectively. Therefore, the dominant inner-shell transition for this ion is the $4d$ - $6p$, which has an average excitation threshold of 245 eV. The transitions from the other metastable levels are similar to those from the ground state. The main difference is in the reduction of the direct ionization cross section as a function of ionization stage. There is an unusual high-energy resonance observed in the experi-

mental spectrum that is due to deep-core dielectronic capture followed by sequential double Auger decay [35]. These resonant processes are currently being studied and will be reported in a later publication.

VI. SUMMARY

In this paper, we have reported on a joint experimental and theoretical study of the electron-impact ionization of Sm^{q+} ions for $q = 1 - 12$. The experimental measurements have been made using the electron-ion crossed-beam apparatus described previously [12], and the theoretical calculations have used a configuration-average distorted-wave approach.

The rare-earth-metal series has, to date, received relatively little attention in electron-impact ionization studies. This is chiefly due to the complexity of the atomic structure, where open $4f$, $5p$, and $4d$ shells provide electron configurations with many thousands of closely spaced levels. This makes detailed level-to-level calculations of ionization and excitation cross sections computationally prohibitive, and thus a configuration-average approach is the only feasible theoretical tool for studying these systems. Furthermore, the accuracy of the configuration-average method improves with the complexity of the atomic system.

Experimentally, studies of the rare-earth-metal series also present difficulties. Due to the number of low-lying complex configurations in these atoms, ion beams tend to consist of undetermined fractions of ions in the levels of the ground and excited configurations. This makes the analysis of the experimental data much more challenging.

The agreement between experiment and theory presented in this paper is reasonably good. The position of the peaks in the ionization cross sections have been well reproduced by theory, and for most of the ions discussed here, the magnitude of the cross sections are in fair agreement.

ACKNOWLEDGMENTS

This work was supported in part by the U.S. Department of Energy, a subcontract from Los Alamos National Laboratory, and the Deutsche Forschungsgemeinschaft (DFG), Bonn Bad-Godesberg. Computational work was carried out at the National Energy Research Supercomputer Center in Oakland, CA.

-
- [1] K. Aichele, U. Hartenfeller, D. Hathiramani, G. Hofmann, V. Schäfer, E. Salzborn, T. Pattard, and J. M. Rost, *J. Phys. B* **31**, 2369 (1998).
- [2] M. Duponchelle, M. Khouilid, E. M. Qualim, H. Zhang, and P. Defrance, *J. Phys. B* **31**, 729 (1997).
- [3] B. Peart and K. Dolder, *J. Phys. B* **1**, 872 (1968).
- [4] R. A. Falk, G. H. Dunn, D. C. Gregory, and D. H. Crandall, *Phys. Rev. A* **27**, 762 (1983).
- [5] D. L. Moores and K. J. Reed, *Adv. At., Mol., Opt. Phys.* **34**, 301 (1995).
- [6] S. S. Tayal and R. J. W. Henry, *Phys. Rev. A* **44**, 2955 (1991).
- [7] D. H. Crandall, R. A. Phaneuf, D. C. Gregory, A. M. Howald, D. W. Mueller, T. J. Morgan, G. H. Dunn, D. C. Griffin, and R. J. W. Henry, *Phys. Rev. A* **34**, 1757 (1987).
- [8] K. J. Reed and M. H. Chen, *Phys. Rev. A* **45**, 4519 (1992).
- [9] C. Y. Chen, S. Yan, Z. Teng, Y. Wang, F. Yang, and Y. Sun, *J. Phys. B* **31**, 2667 (1998).
- [10] M. P. Scott, H. Teng, and P. G. Burke, *J. Phys. B* **33**, L63 (2000).
- [11] A. Müller, G. Hofmann, K. Tinschert, and E. Salzborn, *Phys. Rev. Lett.* **61**, 1352 (1988).
- [12] G. Hofmann, A. Müller, K. Tinschert, and E. Salzborn, *Z. Phys. D: At., Mol. Clusters* **16**, 113 (1990).
- [13] H. Teng, H. Knopp, S. Ricz, S. Schippers, K. A. Berrington,

- and A. Müller, Phys. Rev. A **61**, 060704(R) (2000).
- [14] K. Aichele, W. Shi, F. Scheuermann, H. Teng, E. Salzbom, and A. Müller, Phys. Rev. A **63**, 014701(R) (2000).
- [15] A. M. Howald, D. C. Gregory, F. W. Meyer, R. A. Phaneuf, A. Müller, N. Djuric, and G. H. Dunn, Phys. Rev. A **33**, 3779 (1986).
- [16] D. M. Mitnik, P. Mandelbaum, J. L. Schwob, A. Bar-Shalom, J. Oreg, and W. H. Goldstein, Phys. Rev. A **50**, 4911 (1994).
- [17] R. A. Falk and G. H. Dunn, Phys. Rev. A **27**, 754 (1983).
- [18] B. Peart and K. T. Dolder, J. Phys. B **8**, 56 (1975).
- [19] S. K. Shrivastava and B. N. Roy, J. Phys. B **17**, 4935 (1984).
- [20] A. Müller, K. Tinschert, G. Hofmann, E. Salzbom, and G. H. Dunn, Phys. Rev. Lett. **61**, 70 (1988).
- [21] A. Müller, K. Tinschert, G. Hofmann, E. Salzbom, G. H. Dunn, S. M. Younger, and M. S. Pindzola, Phys. Rev. A **40**, 3584 (1989).
- [22] K. Tinschert, A. Müller, G. Hofmann, E. Salzbom, and S. M. Younger, Phys. Rev. A **43**, 3522 (1991).
- [23] V. A. Komarovskii, Opt. Spektrosk. **71**, 559 (1991).
- [24] K. Tinschert, A. Müller, G. Hofmann, K. Huber, R. Becker, D. C. Gregory, and E. Salzbom, J. Biol. Phys. **22**, 531 (1989).
- [25] R. Becker, A. Müller, C. Achenbach, K. Tinschert, and E. Salzbom, Nucl. Instrum. Methods Phys. Res. B **9**, 384 (1985).
- [26] A. Müller, K. Tinschert, C. Achenbach, and E. Salzbom, Nucl. Instrum. Methods Phys. Res. B **10/11**, 204 (1985).
- [27] M. S. Pindzola, D. C. Griffin, and C. Bottcher, in *Atomic Processes in Electron-Ion and Ion-Ion Collisions*, Vol. 145 of *NATO Advanced Studies Institute Series B: Physics*, edited by F. Brouillard (Plenum Press, New York, 1986).
- [28] R. D. Cowan, *The Theory of Atomic Structure and Spectra* (University of California, Berkeley, 1981).
- [29] M. E. Riley and D. G. Truhlar, J. Chem. Phys. **63**, 2182 (1975).
- [30] J. Oreg, W. H. Goldstein, M. Klapisch, and A. Bar-Shalom, Phys. Rev. A **44**, 1750 (1991).
- [31] M. Klapisch, J. L. Schwob, B. S. Frankel, and J. Oreg, J. Opt. Soc. Am. **67**, 148 (1977).
- [32] M. Klapisch, Comput. Phys. Commun. **2**, 239 (1971).
- [33] W. C. Martin, R. Zalubas, and L. Hagan, *Atomic Energy Levels-The Rare-Earth Elements* (Institute for Basic Standards, Washington, DC, 1978).
- [34] J. Colgan, D. M. Mitnik, and M. S. Pindzola, Phys. Rev. A **63**, 012712 (2000).
- [35] K. Aichele, D. Hathiramani, F. Scheuermann, A. Müller, E. Salzbom, D. Mitnik, J. Colgan, and M. S. Pindzola, Phys. Rev. Lett. **86**, 620 (2001).